AGU PUBLICATIONS

Geophysical Research Letters

RESEARCH LETTER
10.1002/2017GL076380

Key Points:
- The horizontal wind velocity in Venus atmosphere at 90–110 km was obtained from the $O_2(a^1\Delta_g)$ nightglow tracking
- Average zonal component from the morning side exceeds its opposite from the evening side by 20–30 m/s; they "meet" at 22–23 h local time
- The influence of the underlying topography on the wind direction was suggested in some cases

Correspondence to:
D. A. Gorinov,
dmitry_gorinov@rssi.ru

Citation:
Gorinov, D. A., Khatuntsev, I. V., Zasova, L. V., Turin, A. V., & Piccioni, G. (2018). Circulation of Venusian atmosphere at 90–110 km based on apparent motions of the O_2 1.27 μm nightglow from VIRTIS-M (Venus Express) data. *Geophysical Research Letters*, *45*, 2554–2562. https://doi.org/10.1002/2017GL076380

Received 13 NOV 2017
Accepted 20 FEB 2018
Accepted article online 28 FEB 2018
Published online 15 MAR 2018

Circulation of Venusian Atmosphere at 90–110 km Based on Apparent Motions of the O_2 1.27 μm Nightglow From VIRTIS-M (Venus Express) Data

D. A. Gorinov[1], I. V. Khatuntsev[1], L. V. Zasova[1], A. V. Turin[1], and G. Piccioni[2]

[1]Space Research Institute RAS, Moscow, Russia, [2]INAF-IAPS, Rome, Italy

Abstract The paper is devoted to the investigation of Venus mesosphere circulation at 90–110 km altitudes, where tracking of the $O_2(a^1\Delta_g)$ 1.27 μm nightglow is practically the only method of studying the circulation. The images of the nightglow were obtained by VIRTIS-M on Venus Express over the course of more than 2 years. The resulting global mean velocity vector field covers the nightside between latitudes 75°S–20°N and local time 19–5 h. The main observed mode of circulation is two opposite flows from terminators to midnight; however, the wind speed in the eastward direction from the morning side exceeds the westward (evening) by 20–30 m/s, and the streams "meet" at 22.5 ± 0.5 h. The influence of underlying topography was suggested in some cases: Above mountain regions, flows behave as if they encounter an "obstacle" and "wrap around" highlands. Instances of circular motion were discovered, encompassing areas of 1,500–4,000 km.

Plain Language Summary Recent developments in the studies of Venus atmosphere reveal an intriguing phenomenon of stationary gravity waves, which emerge from the surface, interacting with the cloud layer up to ~70 km. In this paper, analysis of the oxygen nightglow on the nightside of Venus using data from VIRTIS instrument (Venus Express spacecraft) delivers clues that the atmosphere at 90–110 km altitude can as well be influenced by such mechanisms. The horizontal motion, obtained from tracking the displacements of the bright features of the nightglow, appears to hold disturbances, the positions of which in some cases coincide with highlands directly below or shifted by several degrees. The nightglow itself, known to manifest an extremely irregular behavior, sometimes repeats the shapes of the mountain ranges below. As another major result, the mean horizontal circulation, calculated for the nightside southern hemisphere, does represent neither superrotation, nor subsolar-to-antisolar circulation, nor a superposition of the two. Both the zonal and the meridional components of the motion have different magnitudes and direction before and after midnight. The results of this research further our knowledge on the upper atmosphere of Venus and pose a challenge for the global circulation models.

1. Introduction

Planet Venus possesses a thick atmosphere which demonstrates a complex combination of motions. The most distinctive dynamic feature of the atmosphere is the zonal superrotation, from near surface levels to 85–90 km in troposphere and mesosphere—a strong and consistent flow that reaches its peak velocity (~100 m × s^{-1}) in low latitudes at altitudes of 65–70 km above the surface (Gierasch et al., 1997; Read, 2013; Zasova et al., 2007) and drops in magnitude in the poleward direction. In thermosphere (>110 km) a subsolar-to-antisolar (SS-AS) circulation cell is driven by the solar heating (Sánchez-Lavega et al., 2017). Thus, the dynamics in the transition region might be influenced by both of these modes (Bougher et al., 2006; Lellouch et al., 1997), as well as other mechanisms, such as gravity waves (Alexander, 1992; Altieri et al., 2014; Bertaux et al., 2016; Peralta et al., 2017; Zhang et al., 1996) and thermal tides (Zasova et al., 2007).

The $O_2(a^1\Delta)$ 1.27 μm nightglow can be a tracer of the circulation in the transition region. Formed on the dayside due to the photolysis of the CO_2 molecules in mesosphere, atomic oxygen travels onto the nightside at 120–140 km with the SS-AS circulation, descends, and recombines in the descending flux into molecular oxygen in the excited ($a^1\Delta_g$) state (Connes et al., 1979; Crisp et al., 1996). The O_2 1.27 μm nightglow was first detected and then observed from Earth (Bailey et al., 2008; Crisp et al., 1996; Connes et al., 1979; Ohtsuki et al., 2005); it was first observed from the images from the infrared channel of the Visible and InfraRed Thermal Imaging Spectrometer (VIRTIS-M) (Drossart, Piccioni, Gérard, et al., 2007; Drossart, Piccioni, Adriani,

et al., 2007; Piccioni et al., 2009) onboard of the Venus Express mission (Svedhem et al., 2009) in 2006–2008. The instrument carried out measurements in both nadir and limb modes. From limb mode observations $O_2(a^1\Delta_g)$ emission vertical profiles were obtained, and the mean altitude of the emission peak was found at 97.4 ± 2.5 km altitude. The double peak, observed in some cases, was interpreted after modeling (Altieri et al., 2014) as gravity waves with vertical wavelength of 10–14 km and horizontal wavelength of 100–1,000 km. The nadir measurements showed the distribution of the emission over the nightside and appearance of the local maxima at different latitudes and local time (LT), but on the averaged map, a wide spread spot of higher intensity of nightglow appeared around midnight (Piccioni et al., 2009; Shakun et al., 2010). In the paper by Shakun et al. (2010), the average emission maximum was found shifted from midnight to 23 h. Several studies on the issue analyzed the high spatial variability of the nightglow, as the bright emission areas appear to be unstable and shift their magnitude and coordinates of the local maxima from orbit to orbit (Gérard et al., 2014; Piccioni et al., 2009; Soret et al., 2014).

Observations of the dayside atomic oxygen emission at 130 nm from Pioneer Venus Orbiter Ultraviolet Spectrometer brought data on the thermosphere structure and circulation at ~95 km altitudes (Alexander et al., 1993). In addition, the results showed evidence of the SS-AS influence at middle and high latitudes (>30°), as well as asymmetry of the atomic oxygen mixing ratio between the morning and the evening terminators. The amount of the evening terminator oxygen atoms was found to be about twice as large as that of the morning terminator. The phenomenon was interpreted as the influence of the SS-AS circulation and the gravity waves propagating upward from the middle atmosphere (Alexander, 1992; Alexander et al., 1993). The asymmetry between terminators was found from Venera-15 Fourier spectrometer data (Zasova et al., 2007) in such a way that, at 95 km altitude, the temperature at the evening terminator was ~20 K lower than that in the morning; it was explained as a result of thermal tide activity. The diurnal and semidiurnal amplitudes were found to reach 6 and 5 K, respectively, at 20–30°N latitude.

Longitudinal variations and the influence of topography on the atmospheric processes have been reported in various studies. Deceleration of wind (Bertaux et al., 2016) observed over Aphrodite Terra was explained through the stationary gravity waves that originate when the horizontal flow interacts with the high elevation topography. The evidence for the stationary wave above Aphrodite Terra comes from the longwave infrared camera (LIR) at 10 ± 2 μm and the ultraviolet imager onboard of Akatsuki spacecraft, which observed the bow-shaped structure (Fukuhara et al., 2017). The influence of the surface topography on dynamic processes in the middle cloud deck was found from dayside near-infrared (1 μm) images obtained by VMC (Venus Monitoring Camera) onboard of Venus Express (Khatuntsev et al., 2017). The influence of surface might manifest an irregular behavior due to the occasional stability of the convective layer between 52 and 57 km (Hauchecorne, 2017). Slowing of the wind speed over the highlands was found from observations in the 3.8 and 5 μm channels (corresponding to 65–70 km altitude) VIRTIS-M and explained by the influence of stationary gravity waves (Peralta et al., 2017). After 1.5 years of LIR/Akatsuki observations the large stationary gravity waves were found dependent not only on longitude but on LT as well (Kouyama et al., 2017).

The "cloud-like" morphology of the oxygen nightglow allows for tracking the displacement of bright features as markers over time, given a set of consecutive images. Hueso et al. (2008) were the first to attempt to track displacements of the oxygen emission features, having analyzed 23 orbits of the VIRTIS M-channel data set. They stated both zonal and meridional components to be highly variable in magnitude and direction and noted the general coincidence of the apparent nightglow motion with the SS-AS mode of circulation, LT asymmetry, and instances of curved flows.

2. Experimental Data and Approach

The method of manual wind tracking used in this work was first implemented with VMC data (Khatuntsev et al., 2013; Moissl et al., 2009). The zonal u and meridional v components of the wind speed are determined from the following equations:

$$u = \frac{(\lambda_2 - \lambda_1)(R + h)\cos(\varphi_1)}{\Delta t}$$

$$v = \frac{(\varphi_2 - \varphi_1)(R + h)}{\Delta t}$$

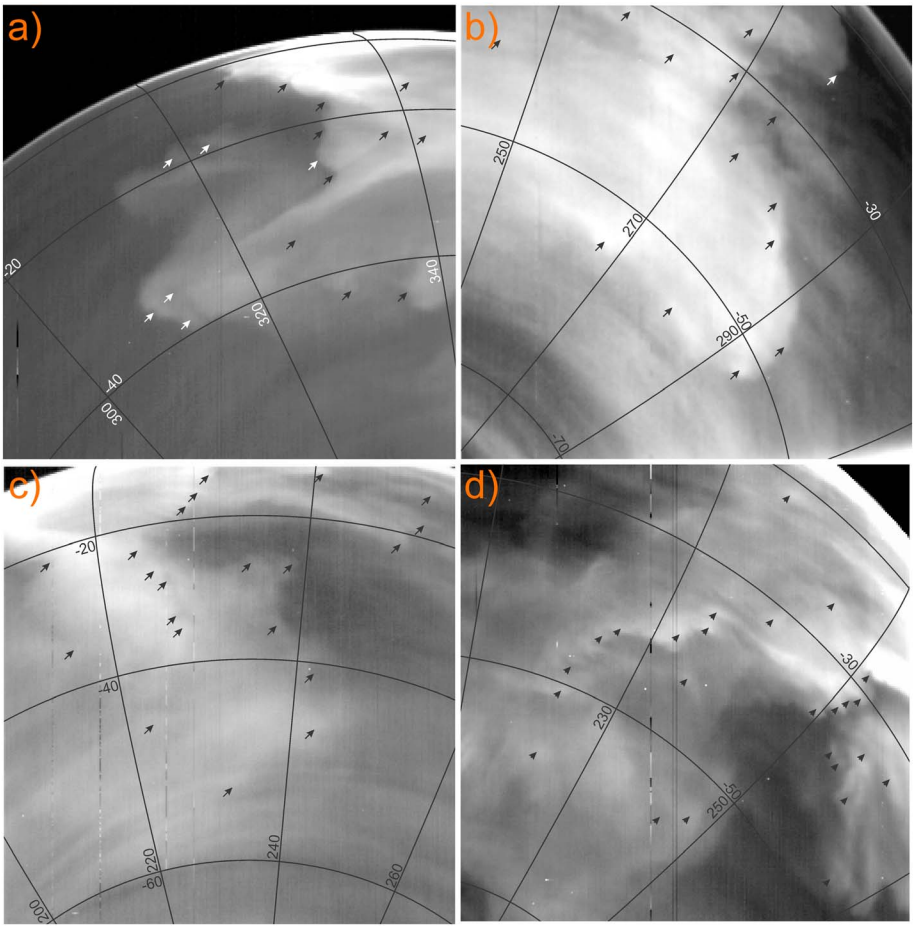

Figure 1. Examples of $O_2(a^1\Delta_g)$ 1.27 μm nightglow images by Visible and InfraRed Thermal Imaging Spectrometer: (a) orbit #0372, cube #01, slant range 66,304 km, 26 April 2007; (b) orbit #0569, cube #05, slant range 65,481 km, 10 November 2007; (c) orbit #0571, cube #04, slant range 66,509 km, 12 November 2007; (d) orbit #0793, cube #01, slant range 64,591 km, 21 June 2008. The arrows indicate traceable cloud features.

where $\lambda_{1,2}$ and $\varphi_{1,2}$ are, respectively, longitudes and latitudes of the tracked airglow features in the first and the second images; R = 6,051.8 km is the radius of Venus; h = 97.5 km is the assumed altitude of the features; and Δt is the time interval between two images.

Figure 1 shows examples of the $O_2(a^1\Delta)$ 1.27 μm nightglow images. The arrows point out instances of the traceable features, which allow tracking of the horizontal wind. We used images taken at a distance of 40,000–67,000 km from the planet with a pixel size of 10–40 km. Each measurement required a pair of consecutive images of the same area of the planet. The time interval between images in pairs varies from 0.5 to 2 h. The large-scale O_2 emission areas are known to exist for many hours (Soret et al., 2014); however, the small-scale traceable features are more variable. Although they are very consistent during 1 h period, within the $(a^1\Delta)$ state radiative lifetime of ~72 min (Miller et al., 2001), some of them (5–15%) may disappear completely or deform in such a way that makes their tracking unreliable, thus lowering the amount of obtained vectors.

Each velocity vector is accompanied by its positioning accuracy, which leads to single measurement errors in the manual tracking method. Throughout the data set, we considered the features that can be displaced while positioning by no more than 2 pixels. The errors vary depending on the geometry conditions, increasing from the center of the visible planetary disk to the limb, due to an increment of the pixel size in the same direction. As this generally corresponds to the South Pole-equator-North Pole direction, the errors are expected to be higher for the equatorial latitudes and lower in the middle and high latitudes. We

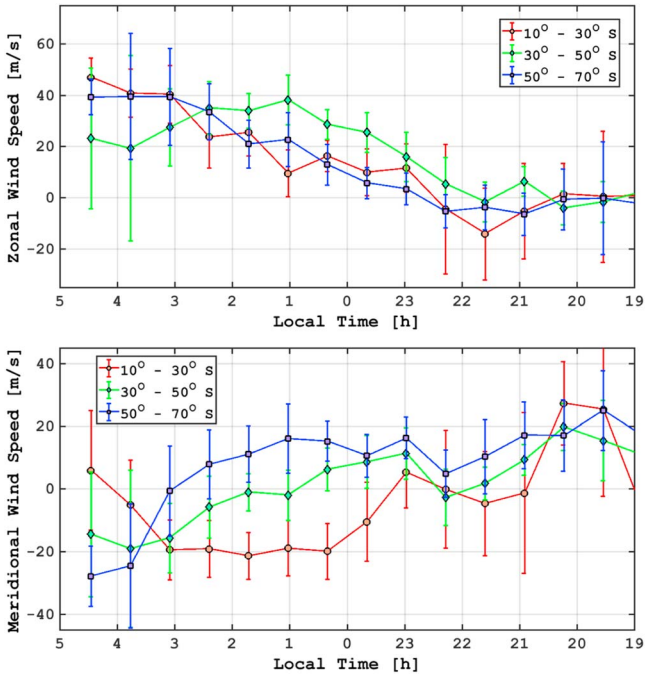

Figure 2. Profiles of mean (a) zonal and (b) meridional components of the horizontal flow at 90–110 km on the nightside of Venus in 20° latitudinal bins. The vertical bars indicate margins of error in a 99% confidence interval. The plus signs of the zonal and meridional components define eastward and northward directions, respectively.

estimated the error for the single measurement of a vector, calculated for two images taken by 1 h between them, to appear in the range between 5–10 m/s in the higher latitudes and 30–40 m/s in the equatorial region. Because of such large errors together with the potential feature distortions the 5–10° area near the limb was avoided during the wind tracking procedure.

In our current work we have analyzed the entire VIRTIS-M channel nadir data set, acquired between July 2006 and September 2008 (orbits 73–861), from which we have chosen 124 orbits that follow our criteria. Tracking of the features have been performed by two operators separately to decrease the human factor in 9,864 measurements.

3. Results

3.1. Local Solar Time Dependence

To obtain the mean maps of both zonal and meridional components in LT-latitude coordinates, the resulting amount of 9,864 vectors was averaged within 7.5° × 0.5 h bins. The results are given in Figure 2. The data coverage of the Venusian night side encompasses the entire southern hemisphere and a part of the northern hemisphere up to 20°N on the morning side. About 80% of all data is positioned between 21–2.5 h and 70°S–15°S.

Both the zonal and meridional components show strong asymmetry in terms of magnitude relative to midnight. The strong zonal component (Figure 2a) on the morning side is directed eastward, opposite to the westward direction that would be observed in the case of the presence of the superrotation, and reaches up to +60 m/s. The westward direction remains between 5 and 22–23 h, with speed gradually decreasing to 0 m/s and changing its direction on the evening side. The evening eastward zonal flow (of the zonal component), however, is significantly weaker than the morning one and does not exceed −30 m/s. The evening zonal motion is more variable and complex and often changes direction from orbit to orbit. The two opposing mean streams "meet" at 21–23 h LT, where the zonal component reaches near-zero values. This asymmetry is in agreement with the results of Hueso et al. (2008).

The meridional component (Figure 2b) is predominantly poleward on the morning side, ranging from 0 to −50 m/s, and changes to equatorward at middle latitudes (>40–50°S, LT < 2 h). On the evening side the meridional component of the wind is mostly equatorward and reaches +40 m/s. In the equatorial latitudes (15°S–15°N) the meridional component is directed toward the South Pole with mean velocities ranging from 0 to −40 m/s. Because both zonal and meridional components are comparable in magnitude, the mean horizontal velocity in 60°S–10°S range on most of the morning side is directed eastward and poleward, and westward and equatorward on most of the evening side.

3.2. Influence of Topography

In order to study variations of the wind we analyzed vector fields measured at individual orbits. For this analysis we only used those orbits where the wind speed was more reliably measured with more than 200 vectors and an area covered my measurements larger than 50° × 50°. Results typically manifest the general behavior described above, that is, two opposing flows from the terminators and the asymmetry relative to 22–23 h LT. However, one can usually see (examples in Figure 3) deviations of the wind direction that coincide with large topographic structures below, mainly highland regions (Atla, Phoebe, etc.). The flows act as if they encounter an "obstacle"—they change direction, wrapping around these areas. In some cases this causes the wind to form areas of curved motion which can range from 1,000 to 4,000 km in diameter.

Examples of horizontal wind vector fields at 90–110 km altitude over the underlying topography for individual orbits are shown on Figure 3. The longitude (180°–20°) and latitude (60°S–5°N) range of the images is

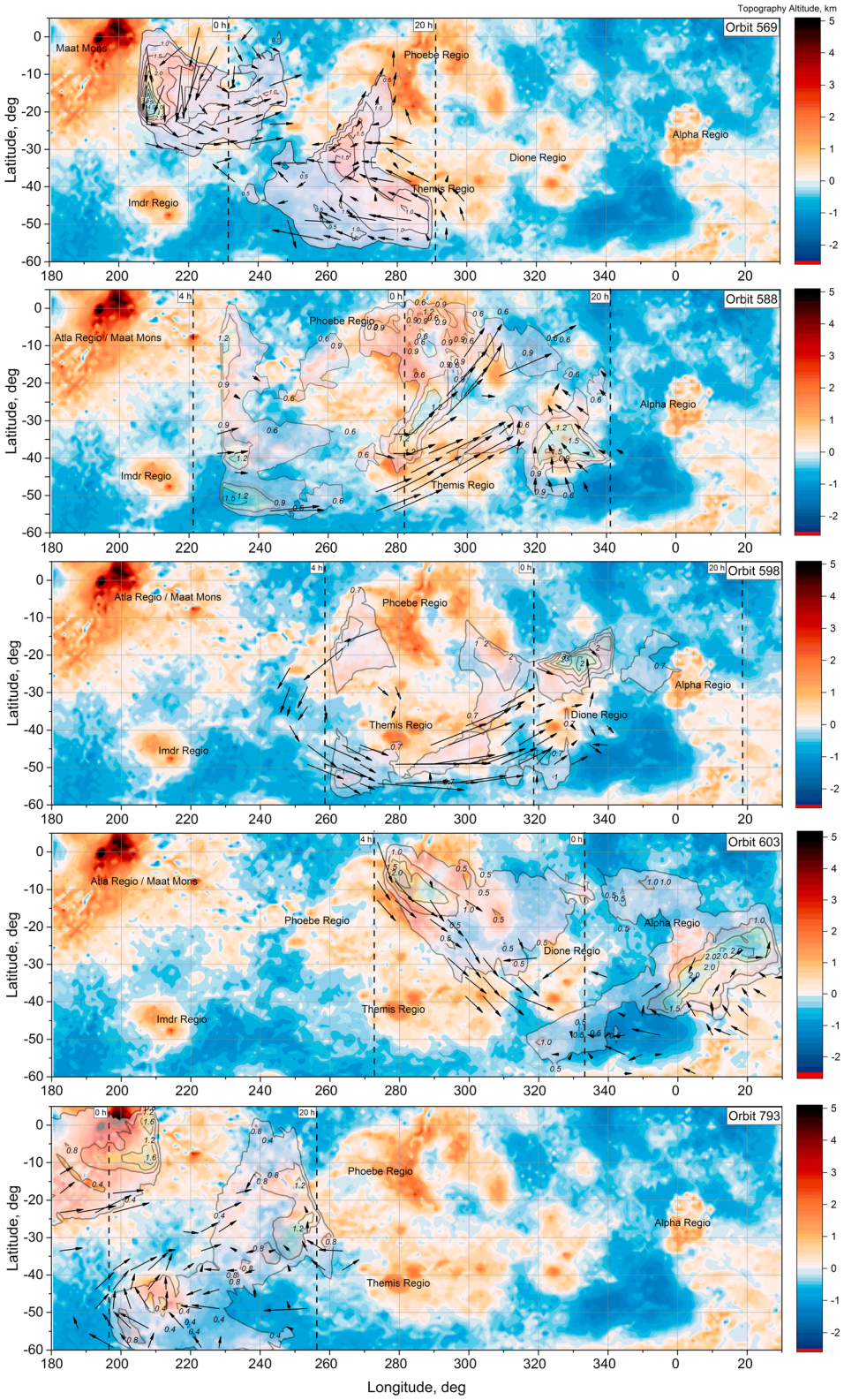

Figure 3. Examples of individual orbit vector fields of horizontal wind flow at 90–110 km altitude over the underlying topography (Magellan global topography data from NASA Planetary Data System, shown as background color). The numbers near isolines indicate the O_2 1.27 μm nightglow intensity in MR. The isolines start from the intensity level of (a and d) 0.5 MR, (b) 0.6 MR, (c) 0.7 MR, (e) 0.4 MR, as to not overload the figure. The arrows represent average apparent atmospheric motion in 5° × 5° bins, where the end of a vector shows where the beginning of the same vector would move over the period of 3 h. The local time for each image is defined by the 20, 0, and 4 h meridians (dashed line).

larger than the area covered by each image. Figure 3a: Orbit 569 is an example of two streams "meeting" at ~22 h and changing direction of the wind above low relief (planitias), as well as a quasi-circular motion within each of them, which "wrap around" the highlands, such as Themis Regio. The morphology of the O_2 emission resembles the shape of corresponding highlands but shifted in the main direction of the mean flow – to midnight, together with the location of the disturbance in the flow. On Figure 3b (orbit 588) one can see a typical meeting of the two opposing streams which can be seen in Figure 2a as the mean zonal speed distribution. The stronger morning eastward motion stretches over the midnight and meets with the weaker evening westward flow at ~22 h LT. The wind direction changes when above lowlands. Figure 3c (orbit 598) shows a large area of counter clockwise circular motion between 0–4 h with a diameter of ~4000 km. The vectors are wrapping around a large topographic structure that includes Phoebe, Themis and Dione Regios. Present on Figure 3d (orbit 603) is a strong flow on the morning side toward the midnight and the South Pole, lodged between Themis and Dione Regios, a weaker midnight—equatorward motion on the evening side—with Alpha Regio acting as an "obstacle." Figure 3e (orbit 793): a near-zero velocity area near 22 h, created by opposing streams; the evening side flow "wraps around" Imdr Regio.

The implied influence of topography cannot be noted in every instance, but in a partial amount of the entire data set. However, as it was shown in the previous part, some examples provide room for the analysis. To prove the topographic influence statistically it would require reliable amount of longitude-latitude data in narrow (0.5–1 h) LT bins, since the LT dependence is shown to be substantial (section 3.1). The VIRTIS-M data do not fulfill this requirement, as the data are relatively sparse and the standard deviation in each bin is too large to make solid conclusions.

Nonetheless, an important step to point out the influence of topography is to take a numerical approach within the acquired data. As it was stated in section 3.2, the areas of bright nightglow in some cases resemble the shape of the underlying highlands, directly above them or shifted in the direction of the main flow. The bright airglow structures are known to emerge in various locations across the nightside, even though, on average, they distribute around the AS point (Gérard, Saglam, et al., 2008). Here we consider the orbit 367, during which the 1.27 μm nightglow was one of the brightest of the entire VIRTIS-M data set, reaching its peak value of ~6 MR. The bright structure was observed between 290° and 320° longitude (0.5–2.5 h LT) and 40°S and 10°N (limb of the disk of Venus) latitude. It can be also observed later during orbits 368–372, as its brightness decreases and it deforms and "drifts." The retrieved velocity vectors show a variety of motion; the main flow, however, is eastward and poleward (Figure 4a), which is typical for the morning side (Figure 2). In the southern part of the image a counter clockwise rotation of the motion was observed.

Assuming the shift of the bright structure in the direction of the main flow and its resemblance to the shape of the Phoebe Regio, we can calculate the correlation between the topography altitudes and the nightglow values. Therefore, the nightglow map needs to be shifted against the main flow and rotated in the clockwise direction. The maximum of the correlation function in a 5° × 5° grid was 0.61 after a 20° westward, 7° equatorward shift, and a 14° clockwise rotation. The diminishing of the correlation coefficient can be attributed to the observed small-scale motions that can deform the bright structure.

4. Discussion and Conclusion

Following our results, the circulation in the transition region on the nightside of Venus appears to be more complex than expected. Two opposing zonal flows emanating from both terminators resemble SS-AS mode of circulation; however, they are asymmetric (zonal asymmetry is in agreement with Hueso et al., 2008) in such a way that the wind speed on the morning side is higher than on the evening side and both flows meet around 22 h, 2 h before midnight, which rules out the influence of retrograde zonal superrotation at those altitudes. The meridional component is also asymmetric, being poleward mostly west of midnight meridian (morning) and on equatorial latitudes and equatorward on the evening side and on higher latitudes, thus not indicating to a strict SS-AS mode of circulation since it is not equatorward at all observed LTs.

After analyzing the wind fields of individual orbits, we found that the asymmetry with respect to the midnight meridian, observed on the global map, usually presents itself at every individual orbit: Both flows meet at 22.5 ± 0.5 h. This is accompanied by the asymmetry of airglow intensity between the terminators: Higher

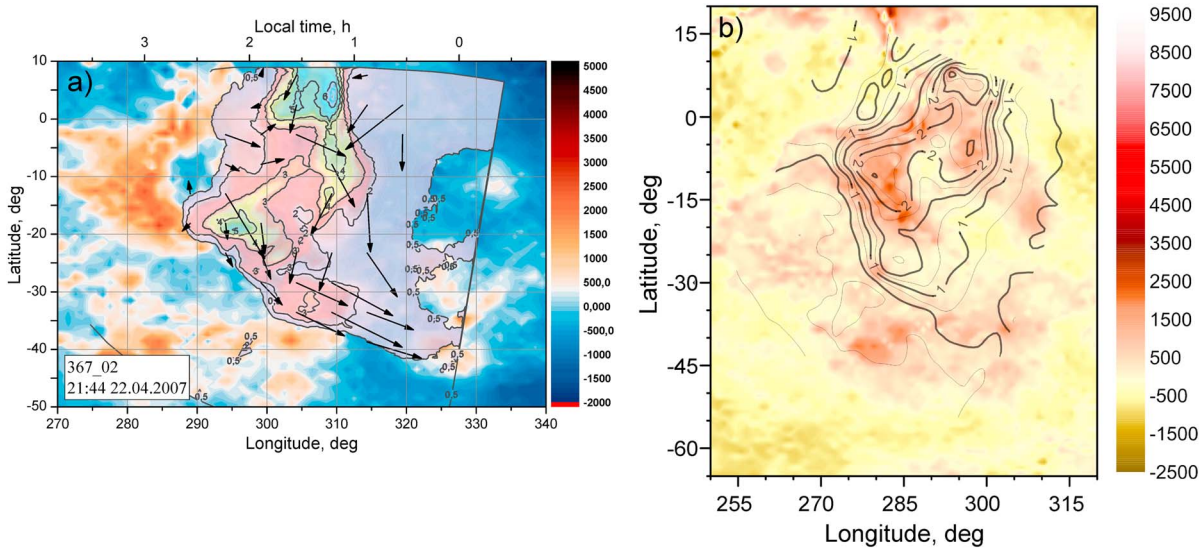

Figure 4. (a) Orbit 367, image 02 in 1.27 μm. The arrows represent retrieved wind velocity vectors in 5° × 5° bins; isolines indicate nightglow levels in MR; Venus topography (Magellan data) is the colored background. (b) Contours from (a) overlaid on Venus topography after a 20° westward, 7° equatorward shift and a 14° clockwise rotation.

intensity is observed at the evening terminator (Gérard, Cox, et al., 2008; Shakun et al., 2010). A higher horizontal flow speed indicates a lower convergence and hence a lower intensity of airglow.

Several other asymmetries in the transition region were discovered previously. The asymmetry of NO distribution in thermosphere was observed by Pioneer Venus (Stewart et al., 1980) and SPICAV (Stiepen et al., 2013). The NO bright spot was observed at 2 h in the morning instead of expected 0 h, and the shift from midnight is explained by the authors as the influence of zonal superrotation in the thermosphere (about 120 km altitude). The asymmetries between terminators were observed at 95 km in atomic oxygen distribution (Alexander et al., 1993)—on the evening terminator, there were twice as many oxygen atoms. This was explained by the influence of gravity waves, propagating from mesosphere. At 95 km altitude the asymmetry in temperature was discovered: The temperature was higher by 15–20 K on the morning terminator, which could be explained as the result of thermal tides (Zasova et al., 2007). None of these cases are applicable directly to explain the asymmetry of the wind speed. Evidently, SS-AS circulation, gravity waves, and thermal tides are all together responsible for a complex picture we obtained from the apparent motion of the O_2 airglow.

Analysis of the individual orbits suggests influence of the underlying topography. The areas of airglow are typically found above mountainous areas, observed directly above or shifted several degrees along the current direction of the wind, often repeating the shape of the highland on the surface. The topographic areas seemingly cause disturbances in the flow, acting as if they were "obstacles." The influence of the surface topography on the upper boundary of clouds was found from VMC data (Bertaux et al., 2016) and the images obtained by LIR camera (10 μm) on Akatsuki, which revealed a bow-shape feature (Fukuhara et al., 2017). All these details were explained through stationary gravity waves above Aphrodite Terra. Later it was shown that bow-shape features can appear and disappear above highlands that generate them. Large stationary gravity waves depend on both topography and LT (Kouyama et al., 2017). The atmosphere of Venus is stable above 60 km; thus, gravity waves may migrate to the transition region and provide signs of topography in the horizontal motion. The areas of strong nightglow emission manifest a variable behavior, often not emerging in the AS point. Stationary gravity waves above high lands could explain the inconsistent emergence of the bright spots and the dynamics around them. Small longitudinal scale of a mountainous region might decrease the potential of generating gravity waves (Kouyama et al., 2017), which can be the reason for inconsistent detection of the influence by Phoebe Regio and similar sized highlands. Recent developments in the global circulation models point out the capability of vertical waves to reach the altitudes of 90–95 km (Mingalev et al., 2015).

Acknowledgments
The authors are grateful to the ESA Mission and Operations teams for flawless operations of the VIRTIS instrument. D.A. Gorinov and I.V. Khatuntsev were supported by the Ministry of Education and Science of Russian Federation grant 14.W03.31.0017. L.V. Zasova and A.V. Turin were supported by the Federal Agency for Scientific Organizations (FASO Russia) grant 0028-2014-0004. The authors thank J.-L. Bertaux for insightful discussion. The authors would like to express gratitude to Takeshi Horinouchi and anonymous reviewers for their comments to the manuscript. The data used are listed in the references, table, figures, and VIRTIS repository at ftp://psa.esac.esa.int/pub/mirror/VENUS-EXPRESS/VIRTIS/. Aforementioned database of wind vectors can be accessed by personal request.

References

Alexander, M. J. (1992). A mechanism for the Venus thermospheric superrotation. *Geophysical Research Letters*, *98*(E6), 10,849–12,210. https://doi.org/10.1029/93JE00538

Alexander, M. J., Stewart, A. I. F., Solomon, S. C., & Bougher, S. W. (1993). Local time asymmetries in the Venus thermosphere. *Journal of Geophysical Research*, *98*(E6), 10,849–10,871. https://doi.org/10.1029/93JE00538

Altieri, F., Migliorini, A., Zasova, L., Shakun, A., Piccioni, G., & Bellucci, G. (2014). Modeling VIRTIS/VEX $O_2(a^1\Delta_g)$ nightglow profiles affected by the propagation of gravity waves in the Venus upper mesosphere. *Journal of Geophysical Research: Planet*, *119*, 2300–2316. https://doi.org/10.1002/2013JE004585

Bailey, J., Meadows, V. S., Chamberlain, S., & Crisp, D. (2008). The temperature of the Venus mesosphere from $O_2(a^1\Delta_g)$ airglow observations. *Icarus*, *197*(1), 247–259. https://doi.org/10.1016/j.icarus.2008.04.007

Bertaux, J.-L., Khatuntsev, I. V., Hauchecorne, A., Markiewicz, W. J., Marcq, E., Lebonnois, S., et al. (2016). Influence of Venus topography on the zonal wind and UV albedo at cloud top level: The role of stationary gravity waves. *Journal of Geophysical Research: Planets*, *121*, 1087–1101. https://doi.org/10.1002/2015JE004958

Bougher, S. W., Rafkin, S., & Drossart, P. (2006). Dynamics of the Venus upper atmosphere: Outstanding problems and new constraints expected from Venus Express. *Planetary and Space Science*, *54*(13-14), 1371–1380. https://doi.org/10.1016/j.pss.2006.04.023

Connes, P., Noxon, J. F., Traub, W. A., & Carleton, P. (1979). $O_2(^1D)$ emission in the day and night airglow of Venus. *Astrophysical Journal*, *233*, L29–L32. https://doi.org/10.1086/183070

Crisp, D., Meadows, V. S., Bézard, B., de Bergh, C., Maillard, J., & Mills, F. P. (1996). Ground-based near-infrared observations of the Venus nightside: 1.27-mm O2(a1Δg) airglow from the upper atmosphere. *Journal of Geophysical Research*, *101*(E2), 4577–4593. https://doi.org/10.1029/95JE03136

Drossart, P., Piccioni, G., Adriani, A., Angrilli, F., Arnold, G., Baines, K. H., et al. (2007). Scientific goals for the observation of Venus by VIRTIS on ESA/Venus Express mission. *Planetary and Space Science*, *55*(12), 1653–1672. https://doi.org/10.1016/j.pss.2007.01.003

Drossart, P., Piccioni, G., Gérard, J. C., Lopez-Valverde, M. A., Sanchez-Lavega, A., Zasova, L., et al. (2007). A dynamic upper atmosphere of Venus as revealed by VIRTIS on Venus Express. *Nature*, *450*(7170), 641–645. https://doi.org/10.1038/nature06140

Fukuhara, T., Futaguchi, M., Hashimoto, G. L., Horinouchi, T., Imamura, T., Iwagaimi, N., et al. (2017). Large stationary gravity wave in the atmosphere of Venus. *Nature Geoscience*, *10*(2), 85–88. https://doi.org/10.1038/ngeo2873

Gérard, J.-C., Cox, C., Saglam, A., Bertaux, J.-L., Villard, E., & Nehmé, C. (2008). Limb observations of the ultraviolet nitric oxide nightglow with SPICAV on board Venus Express. *Journal of Geophysical Research*, *113*, E00B03. https://doi.org/10.1029/2008JE003078

Gérard, J.-C., Saglam, A., Piccioni, G., Drossart, P., Cox, C., Erard, S., et al. (2008). Distribution of the O_2 infrared nightglow observed with VIRTIS on board Venus Express. *Geophysical Research Letters*, *35*, L02207. https://doi.org/10.1029/2007GL032021

Gérard, J.-C., Soret, L., Piccioni, G., & Drossart, P. (2014). Latitudinal structure of the Venus O_2 infrared airglow: A signature of small-scale dynamical processes in the upper atmosphere. *Icarus*, *236*, 92–103. https://doi.org/10.1016/j.icarus.2014.03.028

Gierasch, P. J., Goody, R. M., Young, R. E., Crisp, D., Edwards, C., Kahn, R., et al. (1997). The general circulation of the Venus atmosphere: An assessment. In J. W. Bucher, D. M. Hunten, & R. J. Phillips (Eds.), *Venus II—Geology, geophysics, atmosphere, and solar wind environment* (pp. 459–500). Tucson: University of Arizona Press.

Hauchecorne, A. (2017). Venus: Jet-setting atmosphere. *Nature Geoscience*, *10*(9), 622–623. https://doi.org/10.1038/ngeo3022

Hueso, R., Sanchez-Lavega, A., Piccioni, G., Drossart, P., Gérard, J. C., Khatuntsev, I., et al. (2008). Morphology and dynamics of Venus oxygen airglow from Venus Express/VIRTIS observations. *Journal of Geophysical Research*, *113*, E00B02. https://doi.org/10.1029/2008JE003081

Khatuntsev, I. V., Patsaeva, M. V., Titov, D. V., Ignatiev, N. I., Turin, A. V., Fedorova, A. A., & Markiewicz, W. J. (2017). Winds in the middle cloud deck from the near-IR imaging by the Venus Monitoring Camera onboard Venus Express. *Journal of Geophysical Research: Planets*, *122*, 2312–2327. https://doi.org/10.1002/2017JE005355

Khatuntsev, I. V., Patsaeva, M. V., Titov, D. V., Ignatiev, N. I., Turin, A. V., Limaye, S. S., et al. (2013). Cloud level winds from the Venus Express Monitoring Camera imaging. *Icarus*, *226*(1), 140–158. https://doi.org/10.1016/j.icarus.2013.05.018

Kouyama, T., Imamura, T., Taguchi, M., Fukuhara, T., Sato, T. M., Yamazaki, A., et al. (2017). Topographical and local time dependence of large stationary gravity waves observed at the cloud top of Venus. *Geophysical Research Letters*, *44*, 12,098–12,105. https://doi.org/10.1002/2017GL075792

Lellouch, E., Clancy, T., Crisp, D., Kliore, A., Titov, D., & Bougher, W. (1997). Monitoring of mesospheric structure and dynamics. In S. W. Bougher, D. M. Hunten, & R. J. Philips (Eds.), *Venus II: Geology, geophysics, atmospheres, and solar wind environment* (pp. 295–324). Tucson: University of Ariz. Press.

Miller, H. C., McCord, J. E., Choy, J., & Hager, G. D. (2001). Measurement of the radiative lifetime of O2 (a1Δg) using cavity ring down spectroscopy. *Journal of Quantitative Spectroscopy & Radiative Transfer*, *69*(3), 305–325. https://doi.org/10.1016/S0022-4073(00)00086-8

Mingalev, I., Rodin, A., & Orlov, K. (2015). Numerical simulations of the global circulation of the atmosphere of Venus: Effects of surface relief and solar radiation heating. *Solar System Research*, *49*(1), 24–42. https://doi.org/10.1134/S0038094614060057

Moissl, R., Khatuntsev, I., Limaye, S. S., Titov, D. V., Markiewicz, W. J., Ignatiev, N. I., et al. (2009). Cloud top winds from tracking UV features in Venus Monitoring Camera images. *Journal of Geophysical Research*, *114*, E00B31. https://doi.org/10.1029/2008JE003117

Ohtsuki, S. N., Iwagami, N., Sagawa, H., Kasaba, H., Ueno, Y., & Imamura, M. (2005). Ground-based observations of Venus 1.27-μm O_2 airglow. *Advances in Space Research*, *36*, 2038–2042. https://doi.org/10.1016/j.asr.2005.05.078

Peralta, J., Hueso, R., Sánchez-Lavega, A., Lee, Y. J., García-Muñoz, A., Kouyama, T., et al. (2017). Stationary waves and slowly moving features in the night upper clouds of Venus. *Nature Astronomy*, *1*, 0187.

Piccioni, G., Zasova, L., Migliorini, A., Drossart, P., Shakun, A., García Muñoz, A., et al. (2009). Near-IR oxygen nightglow observed by VIRTIS in the Venus upper atmosphere. *Journal of Geophysical Research*, *114*, E00B38. https://doi.org/10.1029/2008JE003133

Read, P. L. (2013). The Dynamics and Circulation of Venus Atmosphere. *Towards Understanding the Climate of Venus, ISSI Scientific Report Series*, *11*. https://doi.org/10.1007/978-1-4614-5064-1_6

Sánchez-Lavega, A., Lebonnois, S., Imamura, T., Read, P., & Luz, D. (2017). The atmospheric dynamics of Venus. *Venus III*, 1541–1616.

Shakun, A. V., Zasova, L. V., Piccioni, G., Drossart, P., & Migliorini, A. (2010). Investigation of oxygen $O_2(a^1\Delta_g)$ emission on the nightside of Venus: Nadir data of the VIRTIS-M experiment of the Venus Express mission. *Cosmic Research*, *48*(3), 232–239. https://doi.org/10.1134/S0010952510030044

Soret, L., Gérard, J.-C., Piccioni, G., & Drossart, P. (2014). Time variations of $O_2(a^1\Delta)$ nightglow spots on the Venus nightside and dynamics of the upper mesosphere. *Icarus*, *237*, 306–314. https://doi.org/10.1016/j.icarus.2014.03.034

Stewart, A. I. F., Gérard, J.-C., Rusch, D. W., & Bougher, S. W. (1980). Morphology of the Venus ultraviolet night airglow. *Journal of Geophysical Research*, *85*(A13), 7861–7870. https://doi.org/10.1029/JA085iA13p07861

Stiepen, A., Gérard, J.-C., Dumont, M., Cox, C., & Bertaux, J.-L. (2013). Venus nitric oxide nightglow mapping from SPICAV nadir observations. *Icarus*, *226*(1), 428–436. https://doi.org/10.1016/j.icarus.2013.05.031

Svedhem, H., Titov, D. V., Taylor, F. W., & Witasse, O. (2009). The Venus Express mission. *Journal of Geophysical Research*, *114*, E00B33. https://doi.org/10.1029/2008JE003290

Zasova, L. V., Ignatiev, N. I., Khatuntsev, I. V., & Linkin, V. M. (2007). Structure of the Venus atmosphere. *Planetary and Space Science*, *55*(12), 1712–1728. https://doi.org/10.1016/j.pss.2007.01.011

Zhang, S., Bougher, S. W., & Alexander, M. J. (1996). The impact of gravity waves on the Venus thermosphere and O_2 IR nightglow. *Journal of Geophysical Research*, *101*(E10), 23,195–23,205. https://doi.org/10.1029/96JE02035